Preparation and Characterization of $SrFe_{12}O_{19}$/ $Ba_2Co_2Fe_{12}O_{22}$ Composite Hexaferrite

Dissertation submitted in partial fulfillment of the requirement for the Degree of

MASTER OF SCIENCE

BY

Pretty Singla

(302104006)

Under the Supervision of

Dr. PUNEET SHARMA

(Professor)

School of Physics & Material Science,

Thapar Institute of Engineering & Technology (TIET), Patiala - 147004

PUNJAB

CERTIFICATE

I hereby certify that the present work in thesis '**Preparation and Characterization of $SrFe_{12}O_{19}$/ $Ba_2Co_2Fe_{12}O_{22}$ composite hexaferrite**' in the partial fulfillment of the requirement for the award of the degree of Master of Science (M. Sc.) in Physics in School of Physics and Materials Science, Thapar Institute of Engineering & Technology, Patiala is an authentic record of my own work carried out under the supervision of Dr. Puneet Sharma. The matter embodied in this thesis has not been submitted in part or full to any other institute/university for the award of any degree.

Pretty Singla

(302104006)

This is to certify that the above mentioned statement of the student is correct to the best of my knowledge and belief.

Dr. Puneet Sharma

Professor

School of Physics & Material Science

Thapar University, Patiala (147004)

Date: 28th July, 2023

ACKNOWLEDGMENT

Foremost, I would like to express my sincere gratitude to **Dr. Puneet Sharma**, Professor (SPMS), for giving me an opportunity to work under his supervision, without whose help and constant guidance this thesis would have not taken place. I am extremely thankful to **Prof. Kulvir Singh**, Head (SPMS) for their co-operation and encouragement. I am also thankful to all the members of SPMS for their constant co-operation during experimental work.

I am highly thankful to **Sonal Singh, Anupriya Choudhary**, **Parminder Singh,** and **Hemanita Sharma** research scholars SPMS, who provided their valuable guidance and suggestions during the work. I acknowledge and thank to my elders, friends and fellow classmates for their support and constant motivation. Last but not least, I am very thankful to my parents for their constant support, patience and blessings.

Table of Contents

List of Figures

List of Tables

List of Flowcharts

Abstract

In the present work, composites of $SrFe_{12}O_{19}$ (SrM)/$Ba_2Co_2Fe_{12}O_{22}$ (Co_2Y) in different weight ratio (98/2, 96/4, 94/6, 92/8) were prepared. Their structural, morphological and magnetic properties were investigated using various techniques; viz. X-ray diffraction (XRD), Field Emission Scanning Electron Microscope (FE-SEM), Raman Spectroscopy and Vibrating Sample Magnetometer (VSM). X-ray diffraction pattern confirmed the co-existence of both phases in composites which is also supported by Raman analysis. The magnetic measurements show non-linear rise in saturation magnetization with the Co_2Y content, while the coercivity drastically decreases. Smooth demagnetization curve of sintered composites confirmed the well-exchange coupling between M-Y phases within the studied composition range.

Chapter 1

Introduction

Overview

This chapter provides a general introduction to ferrites and their crystal structures. Classification of ferrites based upon magnetic and structural properties has been described. A brief description about exchange coupling and exchange-spring mechanism are given. Some important applications of exchange coupled composites are mentioned. The chapter concludes with the motivation and objectives for the present work.

1.1 Ferrites

Ferrites are ceramic materials composed of iron oxide (Fe_2O_3) along with other metal oxides having general chemical formula $A(Fe_xO_y)$, where A(divalent ion): Co, Zn, Ni, Ba, or Sr[1]. They were first investigated by Snoek et. al in 1930's[2]. Ferrites are known for their high electrical resistivity and minimal eddy current losses, which makes them plausible candidate for use in high-frequency electromagnetic fields, permanent magnets, magnetic sensors, etc[3].

Based on magnetic characteristics ferrites are classified as soft and hard ferrites. Soft ferrites have a low coercive force and are easily magnetized and demagnetized, making them ideal for use in electrical device applications. Whereas, hard ferrites have a high coercive force and are difficult to magnetize and demagnetize; which makes them suitable for use in permanent magnets [4]. Further on the basis of their crystal structure, Spinel and garnet ferrites (cubic), hexaferrites (hexagonal), and orthoferrites (perovskite) are the four major types of ferrites. [5].

Table 1.1: Classification of ferrites based on their magnetic and microwave properties

Crystal Structure	Type	Example	Ms (G)	Hc (Oe)	Ha (Oe)	Operable Frequency (GHz)
Cubic	Spinels	$NiFe_2O_4$	3200			0.750
		$CoFe_2O4$	5300	1566	6800	
	Garnets	$Y_3Fe_5O_{12}$	1750		82	<1
Hexaferrites	M	$BaFe_{12}O_{19}$	4000	3187	17460	Upto 36
		$SrFe_{12}O_{19}$	4320	3193	20000	
	Y	$Ba_2Co_2Fe_{12}O_{22}$	2300	60	28,000	Upto 14
	Z	$Ba_3Co_2Fe_{24}O_{41}$	3390	23	12000	1.3
	X	$Ba_2Me_2Fe_{28}O_{46}$	3400	50	9500	3
	W	$BaMe_2Fe_{16}O_{27}$	4800	80	21000	3
	U	$Ba_4Co_2Fe_{36}O_{60}$	4200	2600	10000	30
Orthoferrites	Pervoskite	$GdFeO_3$	5035	729		

Spinels and Garnets are traditional ferrites having cubical crystal symmetry which leads to low magnetocrystalline anisotropy (H_a) and restricts their operational frequency below 3 GHz, however with substitution their application can be enhanced above X band [6].

On the other hand, the hexagonal crystal symmetry of hexaferrites leads to high H_a due to which they are commonly employed in high frequency application devices such as microwave absorbers, antenna substrates as well as in non-reciprocal devices[7].

1.2 M-type ferrite

Among the family of hexaferrites, M-type-ferrites also known as magnetoplumbite have received substantial interest in recent decades due to their remarkable properties, which include extremely high coercivity(H_c), saturation magnetization(M_s), and strong magnetic uniaxial anisotropy along the *c*-axis which makes them suitable candidate for microwave absorbers in the GHz range[8,9]. Their general chemical formula is $MFe_{12}O_{19}$, where M: Ba, Sr and Pb. The crystal structure of these ferrites consists of spinel blocks containing two oxygen layers separated by a hexagonal block containing the divalent ion. It is denoted as RSR*S*, where R denotes hexagonal symmetry and S spinel structure. The asterisk (*) represents the structure's 180° rotation [10]. In the unit cell of M-type hexaferrites, Fe^{+3} ions situated at various crystallographic sites i.e. octahedral, tetrahedral and hexahedral, in which 12k,2a,2b sites are spin up whereas 4f1 and 4f2 are spin down, which are responsible for the net magnetization which is approximately 40 μB[11].

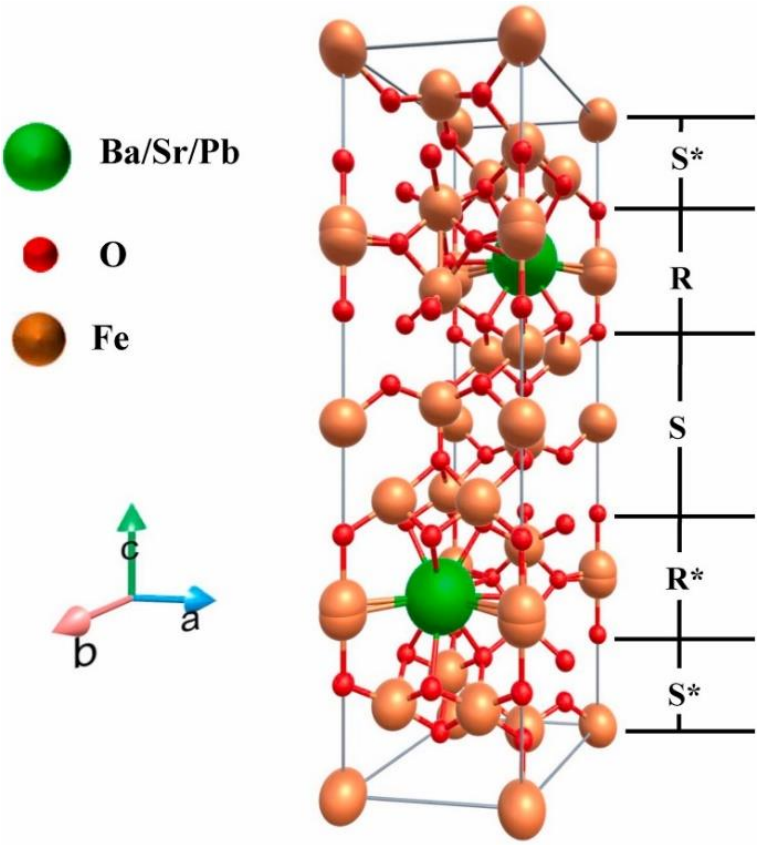

Fig. 1.1 Crystal structure of M-type hexaferrite [10].

1.3 Y-type ferrite

The first ferroxplana ferrites to be found were the Zn_2Y and Co_2Y ferrites, all Y-type ferrites preferred plane of magnetization perpendicular to the *c*-axis at room temperature. These ferrites have chemical formula $Ba_2Me_2Fe_{12}O_{22}$, where Me is a divalent cation[12]. As illustrated in fig. 1.2, one hexagonal unit cell of Y-type has just S and T blocks. The T block is stacked at the bottom of the unit cell, and the S block is piled on top of it. A T* block (the asterisk (*) indicates a 120° rotation along the *c*- axis) and a S** block are piled on top of the first two blocks. S and T blocks are layered to form the unit cell of Y-type hexaferrite[13]. Among the hexaferrites they are a type of soft ferrites with high magnetic permeability and low dielectric losses, making them a viable

high-frequency material for novel chip electronic components including multi-layer chip inductors (MLCI) and multi-layer chip beads (MLCB)[14].

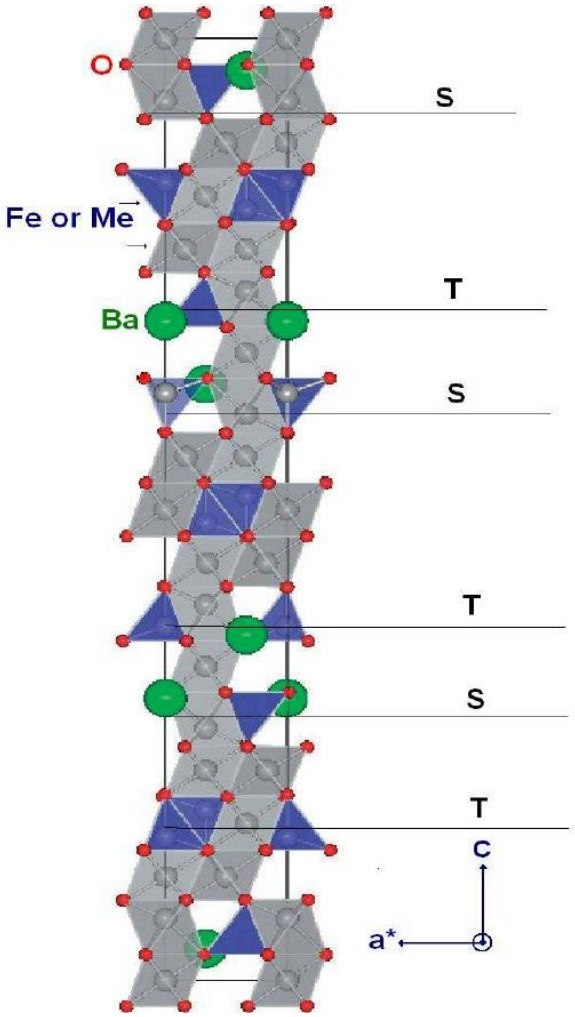

Fig. 1.2 Crystal structure of $Ba_2Me_2Fe_{12}O_{22}$ [11].

1.4 Exchange-coupled composite ferrites

Recently, there has been a surge of interest in the exchange-coupled composites due to the vast difference in the characteristics of various types of ferrites, the composites enhanced remanence and high energy product $(BH)_{max}$ which makes them used as permanent magnets[15]. In the early

1990s, Kneller and Hawing were the first to present the notion of exchange-spring magnets in hard and soft magnetic materials [16].

The exchange-spring phenomena is defined as the interaction of hard and soft magnetic spins at the interface. In 2003, V.M Chakka et al.[17] explained these interactions by using two types of spin reversal mechanisms i.e. coherent and non-coherent. If the two phases are strongly coupled, a coherent rotation of spins occurred at the interface which makes smooth hysteresis curve. In contrast, a stepped *M-H* loop denotes an uncoupled system, in which the rotation of spins are non-coherent at the interface. As exchange coupling is interfacial in nature, it is greatest near the interface and gradually decreases with distance away from the contact. The distance up to which exchange coupling predominate is referred to as exchange length.

In the case of nanoparticles, coupling is highly influenced by particle size distribution whereas in the case of thin films, the quantity of coupling is governed by the thickness of the film [18]. Many aspects, including as synthesis technique and annealing temperature, influence the coupling phenomena.[19]. As a combination of high and low FMR phase, composite ferrites are useful material which operates across a wide frequency range.

1.5 Synthesis methods for ferrites

Ferrites are synthesized using several processing techniques because their electrical and magnetic properties are extremely vulnerable to the synthesis methods. The following are some of the most widely used techniques.

- Solid-state ceramic route
- Sol- gel auto combustion method
- Hydrothermal synthesis
- Chemical co-precipitation

In the present study, composites of SrM and Co_2Y were synthesized via solid-state ceramic route. The experimental section explains the synthesis mechanism.

1.6 Applications of Exchange-Coupled composite ferrites:

Exchange-coupled composite ferrites have emerged as versatile materials with various applications. Their unique magnetic properties and exchange coupling behavior open up a range of possibilities for their utilization. The interaction of hard and soft magnetic phases improves magnetic stability and noise reduction in magnetic recording medium such as hard disc drives (HDDs) and magnetic tapes, resulting in increased data storage and retrieval capabilities[20]. In microwave devices, exchange-coupled composite ferrites find use in circulators, isolators, and phase shifters[21]. Their exchange coupling behavior enables efficient control and manipulation of microwave signals, facilitating effective signal routing and isolation in communication systems[10]. Moreover, these ferrite composites have potential in magnetic sensors, offering improved sensitivity and selectivity in detecting magnetic fields for applications such as position sensing, proximity detection, and non-destructive testing[22]. Furthermore, exchange-coupled composite ferrites show potential in biological applications such as magnetic hyperthermia therapy, where their magnetic characteristics can be used to selectively target and destroy cancer cells.[23].

1.7 Motivation

Modern microwave ferrites have piqued the interest of the microwave sector because of their distinctive electrical and magnetic properties. However, low anisotropic ferrites with low FMR can only be used in the MHz range, whereas high FMR ferrites can be used in the GHz range. As a result, current emphasis has been placed on composite ferrites, which may be used throughout a large frequency spectrum. Several studies have reported exchange coupling between hard/soft composites, but no data on hard/hard composites are known. The structural and magnetic properties of composites of $SrFe_{12}O_{19}/Ba_2Co_2Fe_{12}O_{22}$ in weight ratios of 98/2,96/4,94/6, and 92/8 were examined in this study.

1.8 Objectives

1. Preparation of $SrFe_{12}O_{19}$ /$Ba_2Co_2Fe_{12}O_{22}$ composite of various weight ratio.
2. To investigate the effect of compositional parameters on structural and magnetic properties of M+Y composite ferrites.

Chapter 2

Literature Review

Overview

Large amount of research has been carried out to investigate magnetic and structural properties of ferrites. This section briefly addresses the important work done in last few years on M-type, Y-type and composite ferrites, followed by studies on exchange coupled ferrite involving hexaferrite as one of the phase.

2.1 M-type hexaferrites

Among the hexaferrites, Barium and Strontium ferrites have received substantial interest in recent decades due to their distinctive features such as high H_a, H_c, mild M_s, and high FMR frequency. The important studies on pure and substituted strontium hexaferrite are the focus of this section.

In 1996, Zhiqiang Jin et al**.** [24] synthesized SrM hexaferrite by mechanical alloying. It has been found that low-temperature annealing treatment can influence structural change similarly to a protracted milling procedure. M_s of 74.8 emu/g and H_c of 5.6 kOe found in those samples which milled for 30 hours and annealed at 1000 ℃. The results showed little changes in the M_s and H_c of powders can be seen with prolonged annealing, whereas low properties are produced by short annealing times**.** Further in early 20s, Mohammad Naeem Ashiq et al. [25] used chemical coprecipitation method to synthesize $SrZr_xCd_xFe_{12-2x}O_{19}$ (for x =0.0, 0.2, 0.4, 0.6). It has been found that at modest doping levels of x = 0.2 the saturation magnetization increased while the coercivity decreased. The results suggested that synthesized materials are suitable for high-density recording media applications.

Later on, Ebrahim Roohani et al. [26] synthesized ($SrFe_{12-x}Co_xO_{19}$, x = 0 to 1) by sol-gel auto-combustion method. They performed FT-IR which shows the values of characteristic frequencies for the $SrFe_{12-x}Co_xO_{19}$ samples were moved to a lower frequency as the cobalt doping level increased. The results showed the M_s increased with cobalt content up to x = 0.5 and then gradually declined when the dopant concentration was increased further, while the H_c steadily decreased with increasing Co content. To investigate the structural and magnetic characteristics Chaocheng Liu et al. [27] synthesized $SrCo_xTi_xFe_{12-x}O_{19}$ (x=0.00-1.25) via ceramic reaction route in 2019. The results showed M_s increased slowly as a whole, while H_c decreased gradually when x =1.00. According to M(T) data, Co-Ti substitution can successfully lower the sample's T_p and T_c. The

results suggested $SrCo_xTi_xFe_{12-x}O_{19}$ show potential characteristics for use in multilayer inductors. However, J.C. Guzman-Mínguez et al. [8] in 2020 prepared SrM hexaferrite with the addition of SiO_2 and CaO via dry mixing method to maximize the energy product $(BH)_{max}$. They investigated SiO_2 effectively suppress exaggerated grain growth which significantly increases the H_c of the ceramic dense samples. The results showed that the optimal balance between H_c, M_s and density values is achieved by sintering for 4h at 1200 ℃ with a SiO_2 content of 1 wt%. In addition, Raman microscopy shows the presence of hematite phase formation.

In the year 2021, Le-Zhong Li et al**.** [28] synthesized $Sr_{1-x}Y_xFe_{12-x}Co_xO_{19}$ ($0 \leq x \leq 0.50$) via solid-state route to investigate structural and magnetic characteristics. It has been found that porosity of samples increased as the density of sintered samples declined with increasing Y-Co substitution. The results showed that M_s dropped monotonically as the amount of Y-Co substitution increased while the coercivity initially increased till x rises from 0 to 0.20 after which it decreased.

Sachin Kumar Godara et al. [29] prepared $SrZn_xZr_xFe_{12-2x}O_{19}$ (x = 0.00–0.15) to analyze structural as well as magnetic behavior in 2022. Increase in lattice parameter and volume was observed from XRD analysis. Raman spectra showed that crystals are undergoing strain with increasing Zn^{2+}-Zr^{4+} concentration. The results showed that H_c lies in the range from 5164Oe (x = 0.00) to 6210Oe (x = 0.15) and M_s lies between 71.22 and 82.16 emu/g. Thus, the improvement in SrM's magnetic properties after doping with Zn^{2+}-Zr^{4+} may be crucial for applications involving permanent magnets. Jae-Young Choi et al. [30] synthesized (SrM-Al, $SrFe_{12-x}Al_xO_{19}$, $0 \leq x \leq 4$) by solid state reaction method in the same year. They found significant microstructural inhomogeneity and residual strain which corresponds to poor magnetic performance, therefore to encourage phase formation and slow down rapid grain growth, sodium ions were added using a type of NaOH. As

a consequence, the simultaneous addition of Na and Al ions significantly increased the $(BH)_{max}$ of randomly aligned hard magnetic ceramics to 1.23MGOe.

Recently, Xiang Yu et al. [31] used conventional ceramic method to prepare $SrFe_{12-2x}Zn_xSn_xO_{19}$ (x = 0, 0.25, 0.5, 1, 1.5, 2). The larger ionic radii of Zn^{2+}-Sn^{4+} leads to lattice expansion with increasing substitution. It has been observed that saturation magnetization reaches its maximum value, M_s = 77 emu/g, with x = 0.25. The sample's M_s and H_c will drop monotonically when the amount of Zn^{2+}-Sn^{4+} co-substitution is more than or equal to 0.5. Overall, the result suggests $SrFe_{12-2x}Zn_xSn_xO_{19}$ is a prospective high-density magnetic recording candidate when x=0.25.

2.2 Y-type hexaferrites

In early 20s, Yang Bai et al. [32] synthesized Cu, Zn-modified Co_2Y by solid-state ceramic route. XRD analysis shows single phase of modified Y-type hexaferrites formed at low temperature. Magnetic measurements showed increase in M_s and decrease in H_a with the substitution of Zn^{2+} and reduced sintered temperature with the substitution of Cu^{2+}. The results recommended modified Co_2Y had better magnetic characteristics in the hyper-frequency band. To investigate how temperature affects microstructure and magnetic characteristics Nimai Chand Pramanik et al. [33] prepared $Ba_2Co_2Fe_{12}O_{22}$ (Co_2Y) by polymeric sol–gel method in 2006. It has been discovered that microstructure with particle sizes ranging from 130 to 400nm are created at 900°C, which is significantly lower than the solid state approach. The results revealed a range of H_c (130–1566Oe) and M_s (30.9–47.6emu/g) depending upon temperature. The maximum M_s value reported is 47.60 emu/g at 800°C.

M.M. Costa et. al. [34] prepared $Ba_2Co_2Fe_{12}O_{22}$ (Co_2Y) doped with Bi_2O_3 via solid state reaction method in 2011. The parameters of the dielectric impedance were investigated over the frequency

range of 1 Hz to 1 MHz and in the temperature range of 313 to 493 K. In the next year, Rajshree B. Jotania et al. [11] synthesized series of $Sr_2Cu_{2-x}Co_xFe_{12}O_{22}$ (x = 0.0 to 1.0) via chemical co-precipitation technique. XRD analysis shows single phase Y-type hexaferrite formed below 950℃ sintering temperature Dielectric measurements were taken, and a drop in dielectric properties was seen as frequency increased. Results showed that M_s and M_r decreased with the Co doping content.

M. M. Rashad et al. [35] synthesized $Ba_2Co_2Fe_{12}O_{22}$ via two routes, namely sol-gel auto-combustion (SGA) and co-precipitation (CP) method in 2018. It was observed that porosity decresed in CP route. The result shows for the SGA and CP techniques, M_s of 23.64 and 24.37 emu/g and H_c of 417.76 and 280.92 Oe were achieved for samples pre-annealed at 600℃ for 4 h and then annealed at 1000℃ for 2 h, respectively. In the same year, R. Vinaykumar et al. [36] prepared $Ba_{2-x}La_xCo_2Fe_{12-x}Zn_xO_{22}$, (for x= 0.0, 0.1, 0.3 and 0.5) via solid-state route. The value of M_s increased from 32 emu/g in unsubstituted Co_2Y to 47.7 emu/g in x = 0.5 composition, while the H_c also increased with La-Zn substitution. The results concluded La-Zn substitution in Co_2Y ferrite was an excellent approach for increasing its magnetic and dielectric properties.

In-situ polymerization technique was used by G Packiaraj et al. [37] in 2020 to prepare polyaniline-blended $Ba_2Ni_2Fe_{12}O_{22}$ hexaferrite (weight ratios 1:1, 1:2 and 2:1) . It has been found that value of dielectric constants increased in polyaniline-blended Y-type hexaferrite. The value of M_s, H_c and M_r decreased and tuned with polyaniline concentration. Recently in 2022, Yu Gao et al. [38] synthesized Co_2Y using sol-gel method to study the dielectric and magnetic characteristics by varying sintering temperature (T). The single Y-type hexaferrite phase was formed at $T \leq 1200$℃. It was discovered that as temperature increased, the resonance peak of frequency moved from 10.2 GHz to 1.9 GHz. The effective absorption bandwidth reached 7.3 GHz

at 1100°C with a thickness of only 1.4 mm demonstrates remarkable microwave absorption capabilities.

2.3 Composite Ferrites

Composites have gained a lot of attention in recent years because of their incredible microwave applications, and there has been a lot of research done on their magnetic characteristics over the last few decades. This section outlines the work reported thus far.

To study the structural and magnetic properties with heat treatment Xiansong Liu et al. [39] formed $SrFe_{12}O_{19}$ /γ-Fe_2O_3 in 2002. The results revealed that value of H_c= 6015 Oe, M_s =75.6 emu/g and $(BH)_{max}$= 1.87 MGOe has found in the samples treated at 800°C. From the magnetic measurements and the dM plot, the exchange coupling interaction was observed in the sample which treated below 800°C. In 2009, Debangsu Roy et al. [19] synthesized $BaFe_{12}O_{19}/Ni_{0.8}Zn_{0.2}Fe_2O_4$ composite and studied its structural and magnetic properties. The behavior of exchange coupling was investigated at two distinct temperatures: 400 °C and 800 °C. The composite heated at 400 °C has more profound exchange interactions. The presence of a wide region in the second quadrant revealed that chemical preparation along with adequate sintering conditions resulted the development of a magnet with a high $(BH)_{max}$ value**.** Also, Liuyang Zhang et al. [40] used two step co-precipitation method to synthesize $SrFe_{12}O_{19}/CoFe_2O_4$ nanocomposites with core-shell structure. An XRD study revealed a coating of $CoFe_2O_4$ nanoparticles on the surface of $SrFe_{12}O_{19}$ nanoparticle which was also supported by Raman and TEM measurements. The result shows, in composites the magnetic properties found to be decreased while their microwave absorption capabilities improve significantly.

Haibo Yang et al. [18] prepared $BaFe_{12}O_{19}/Y_3Fe_5O_{12}$ nanocomposite via one step chemical method in 2015. SEM images revealed the presence of hexagonal and plate-like grains. It has been found that the largest reflection loss was -40.8 dB at 9.9GHz. One pot solution combustion method was used by S. R. Saeedi Afshar et al. [41] to synthesize $SrFe_{12}O_{19}/Ni_{0.6}Zn_{0.4}Fe_2O_4$ in 2018. The results showed that 90:10 composites had well exchange coupled interaction with maximum M_s of 56emu/g. Hence, with the addition of the Ni-Zn ferrite phase, the H_c of composites dropped from 5143 to 1778 Oe. Microwave measurements for 90:10 composite was carried out at 9.9 GHz; minimum reflection loss was -23.5 dB.

In the year 2019, Farzin Mohseni et al. [42] prepared BaM/Fe_3O_4 core-shell-like nanocomposite via hydrothermal method. The results indicated a 40% increase in M_s and a 75% rise in $(BH)_{max}$ in the BaM/Fe_3O_4 9:1 hard/soft nanocomposite. It has been concluded that synthesized composite employed as permanent magnets in a number of applications, including permanent magnet motors and electrical devices. Chhavi Pahwa et al. [43] synthesized $BaFe_{12}O_{19}/Ni_{0.5}Zn_{0.5}Fe_2O_4$ by sol-gel auto combustion route in different weight ratios. The composite with weight ratio 70/30 showed maximum M_s while decrease in coercivity observed. The maximum RL for annealed samples at 1050 °C was found to be -38 dB.

P. Maltoni et al**.** [44] used one-pot sol–gel route in 2021 to prepare $SrFe_{12}O_{19}/Co_{1-x}Zn_xFe_2O_4$ composite (for x= 0.1, 0.3 and 0.5) having 80/20 hard to soft ratio. Lattice parameter increases with Zn^{2+} content was observed through XRPD analysis. Magnetic measurements showed maximum M_s is $74Am^2/kg$ for x = 0.3 and H_c is 240kA/m. Recently, V. Bilovol et al**.** [45] prepared $(100\text{-}x)SrFe_{12}O_{19}/(x)CoFe_2O_4$ composites using physical mixing method with x= 10, 20, 30 and 40 wt%. XRD analysis confirms the co-existence of both phases for the samples which annealed at 900°C for 3 h. The results showed that composite with 10% $CoFe_2O_4$ has the $(BH)_{max}$ = 10.9

kJ/m^3, this value is nearly 20% greater than the pure $SrFe_{12}O_{19}$. The existence of exchange coupling effect, as confirmed by Henkel plots, explains the improved magnetic characteristics of composite.

Chapter 3

Experimental Details

Overview

In this chapter, details of the processing technique used for the preparation of $SrFe_{12}O_{19}$ (SrM), $Ba_2Co_2Fe_{12}O_{22}$ (Co_2Y) and series of SrM/Co_2Y composite ferrites are explained. Various characterization techniques used for structural, morphological and magnetic measurements of ferrites has been briefly explained.

3.1 Sample Preparation

The preparation of samples has been divided into two sections. At first, pure M-type and Y-type hexaferrites were prepared via solid-state ceramic route. And in second section preparation of composites using as-prepared powders are explained.

3.1.1 Preparation of powders:

Analytical grade Strontium carbonate ($SrCO_3$), Barium carbonate ($BaCO_3$), Cobalt oxide (Co_3O_4) and Iron oxide (Fe_2O_3) were used as precursors. For the synthesis, precursors were weighed in stochiometric amount given below:

$$SrCO_3 + 6Fe_2O_3 \longrightarrow SrFe_{12}O_{19} + CO_2 \qquad (\mathbf{SrM})$$

$$6BaCO_3 + 18Fe_2O_3 + 2\,Co_3O_4 \longrightarrow Ba_2Co_2Fe_{12}O_{22} + 6CO_2 \qquad (\mathbf{Co_2Y})$$

The powders were wet milled in zirconia jar for 3 hours using planetary ball mill. The charge to ball ratio and rpm were kept constant to 1:2 and 100 respectively. As-mixed powders were dried and pelletized using hydraulic press at a pressure of 13 tons. Further the pellets were calcined in tubler furnace. The calcination temperature and time for SrM and Co_2Y were kept 1130℃ for 3 hrs and 1175℃ for 4 hrs, respectively. The heating as well as cooling rate was kept constant to 5 ℃/min. The calcined pellets were pulverized, sieved and again wet milled in tungsten jar for 1 hour with constant charge to ball ratio (1:5) and rpm ~175 using planetary ball mill.

Flowchart 1 Preparation of SrM and Co_2Y powders by solid-state ceramic route

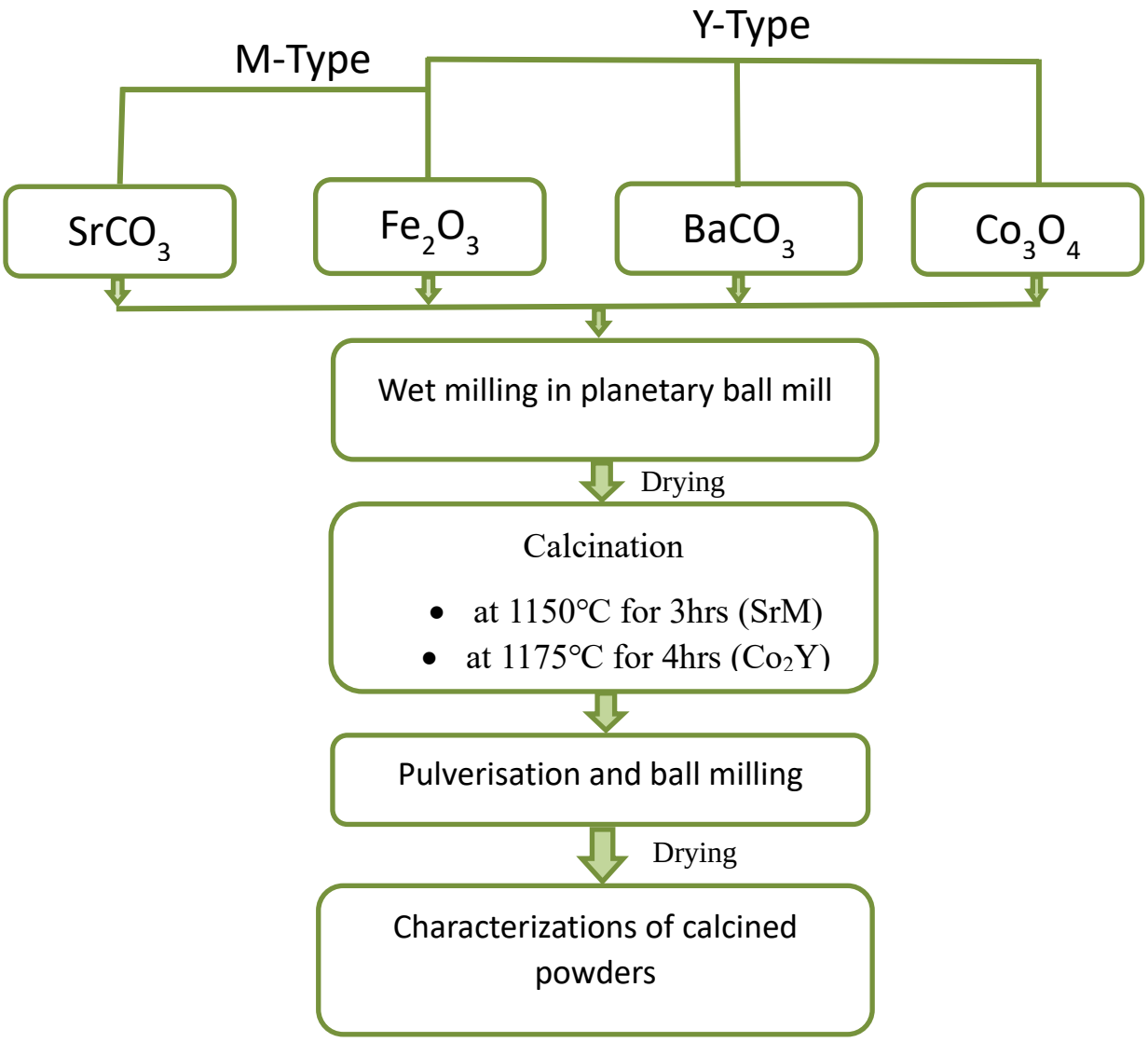

3.1.2 Preparation of SrM/ Co_2Y composites

(1-x)SrM/xCo_2Y (x=0.2,0.4,0.6,0.8) composites were synthesized by mixing as-prepared powders of M- type and Y-type using ball milling for 3 hrs. The charge to ball ratio and rpm were kept constant to 1:2 and 120 respectively.

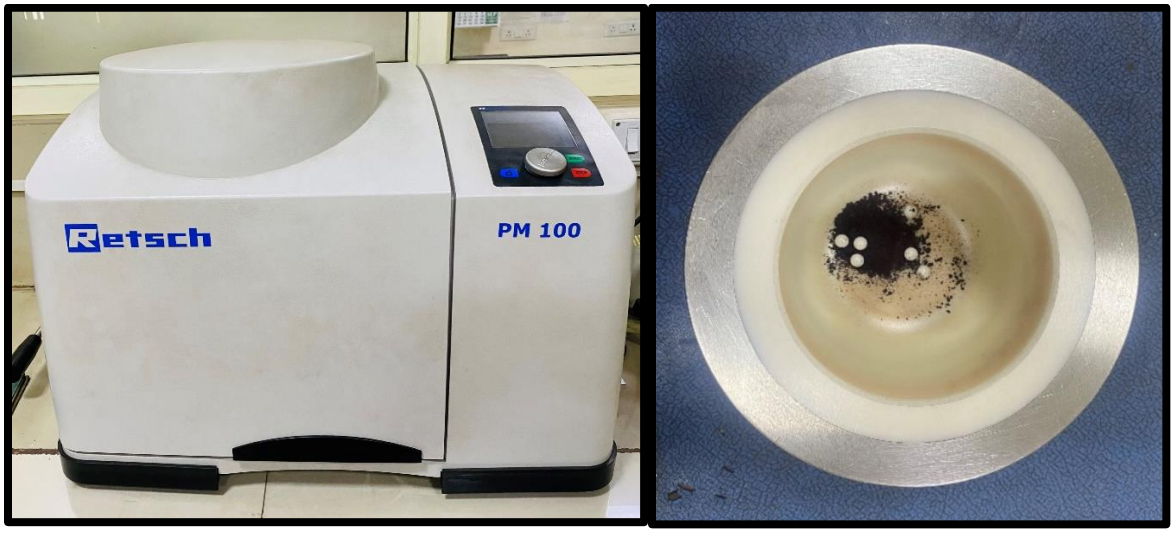

Fig. 3.1 Planetary Ball mill and Zirconia jar with M-Y sample.

Further, the powder was mixed with 5 wt % PVA binder and dried. The dried powder was pelletized using hydraulic press. These pellets were sintered in a muffle furnace for 1 h at 1200 ºC. After sintering, the pellets were pulverized, sieved and wet milled using tungsten jar for 1 hour with constant charge to ball ratio (1:5) and rpm ~175 in planetary ball mill.

Flowchart 2 Preparation of SrM/Co_2Y composites.

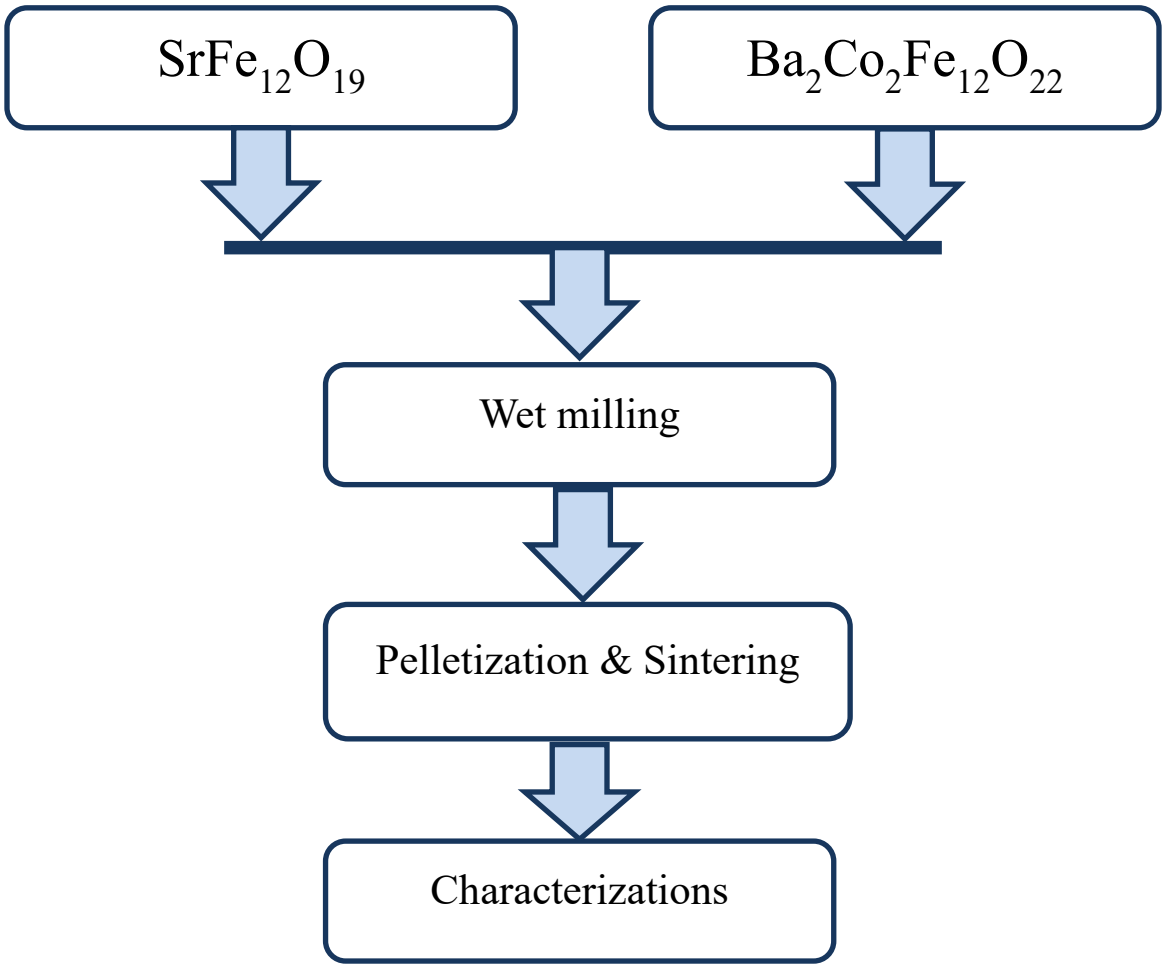

3.2 Characterization technique:

The structural, morphological and magnetic properties of SrM, Co_2Y and SrM/Co_2Y composites were analyzed using following techniques:

1. **X-ray Diffractometer**

   Rigaku SmartLabSE XRD instrument was used to study the phase formation in SrM, Co_2Y and SrM/Co_2Y composites. The phase analysis was performed at room temperature in a scanning range of 20°-80° (2θ) and step size of 0.02°.

2. **Raman Spectroscopy**

   Raman Spectroscopy was carried by Labram HR Confocal Micro-Raman Spectrometer equipped with 532nm laser. The spectral signature obtained from Raman spectroscopy were deconvoluted by Lorentzian fit to verify different Raman active modes.

3. **Field Emission Scanning Electron Microscope:**

   Surface morphology of SrM, Co_2Y and SrM/Co_2Y composites was determined using Carl Zeiss Sigma 500 FEG-SEM instrument. Before measuring, the sample surface was sputtered with gold to prevent sample charging induced by static field accumulation.

4. **Vibrating Sample Magnetometer:**

   The magnetic characteristics of SrM, Co_2Y, and SrM/Co_2Y composites were investigated using the Lake Shore 7404 VSM instrument. At room temperature, a magnetic field in -1 tesla to +1 tesla range was applied.

Chapter 4

Results and Discussions

Overview

Firstly, XRD analysis of SrM, Co_2Y and their compositions were discussed. Further, FE-SEM and Raman analysis was performed to investigate microstructure and lattice vibrations of SrM, Co_2Y and their compositions**.** Lastly, the magnetic behavior of powder and composite was investigated using Vibrating Sample Magnetometer (VSM).

4.1 X-Ray Diffraction (XRD)

XRD patterns of pure SrM, Co_2Y and SrM/Co_2Y composite ferrites in different weight ratios (98/2, 96/4, 94/6, 92/8) are shown in fig. (4.1). All diffraction peaks in SrM and Co_2Y ferrite corresponds to hexagonal phase which are well matched with standard ICDD card no. #01-079-1412, #00-044-0206. In SrM/Co_2Y composites with weight ratio 98/2 and 96/4 all diffraction peaks correspond to M-type and Y-type phase peaks are not identified due to its low content increasing the Y content to 6% (94/6) and 8% (92/8) characteristics peak of Co_2Y is appeared., which confirms the co-existence of both phases.

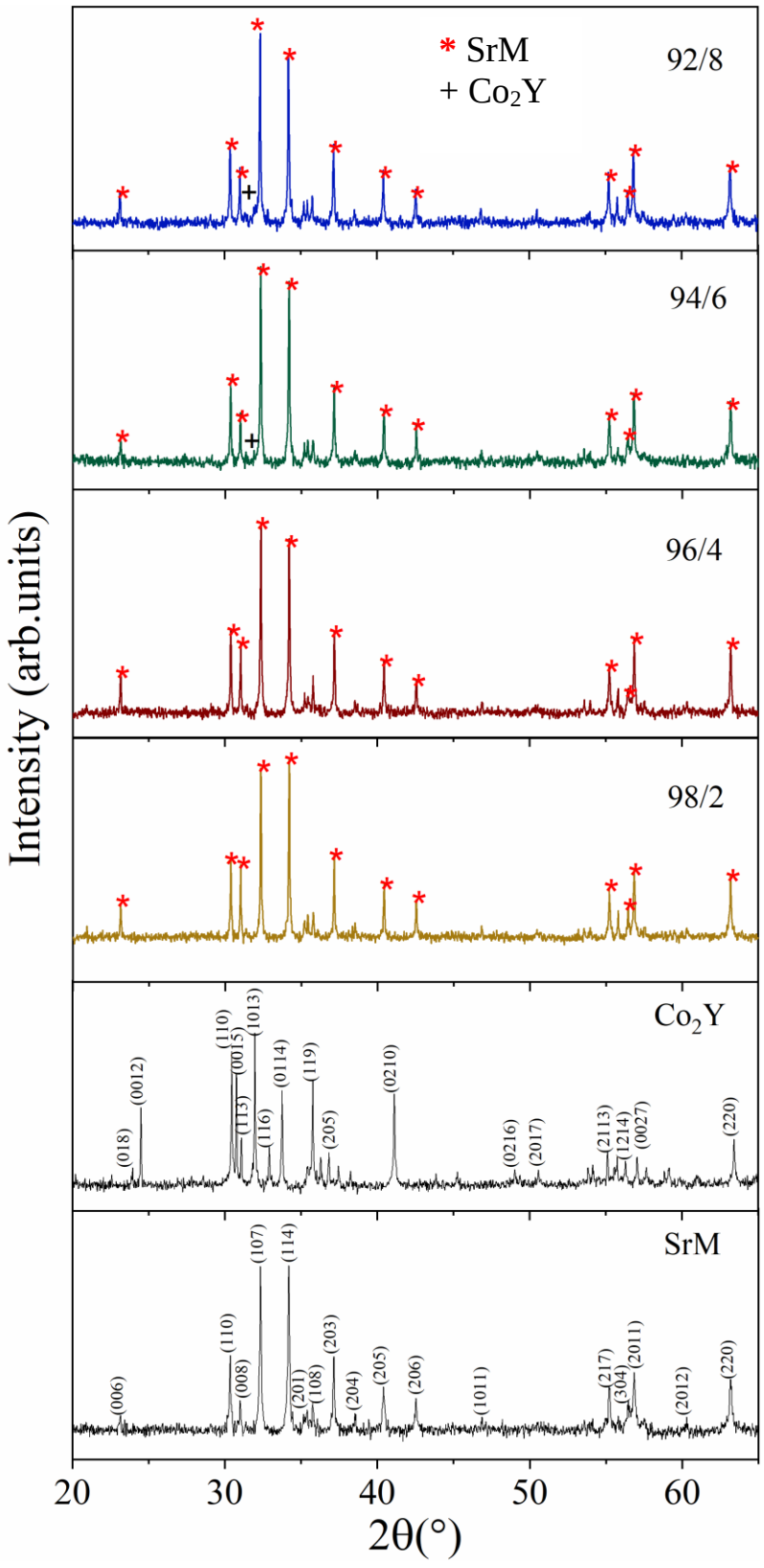

Fig 4.1 X-ray diffraction pattern of pure SrM, pure Co_2Y and SrM/Co_2Y composites.

4.2 Field Emission Scanning Electron Microscope (FE-SEM)

Fig. 4.2 represents surface morphology of SrM, Co_2Y and SrM/Co_2Y composite ferrites in different weight ratios sintered at 1200°C. Micrographs of pure SrM, and Co_2Y showed densely packed well separated grains with hexagonal morphology. The Y-type hexaferrite shows relative larger grain than M-type ferrite, this suggested that the sintering temperature is sufficiently high for in-plane grain growth. In composites, grains are not well separated as in pure ferrites, which may due to the competitive pinning and growth mechanism between both the phases. Moreover, it is difficult to distinguish among the phase due to it similar grain morphology and elements. It is notable that with increasing Y-type phase content, the fraction of large platelets are increasing.

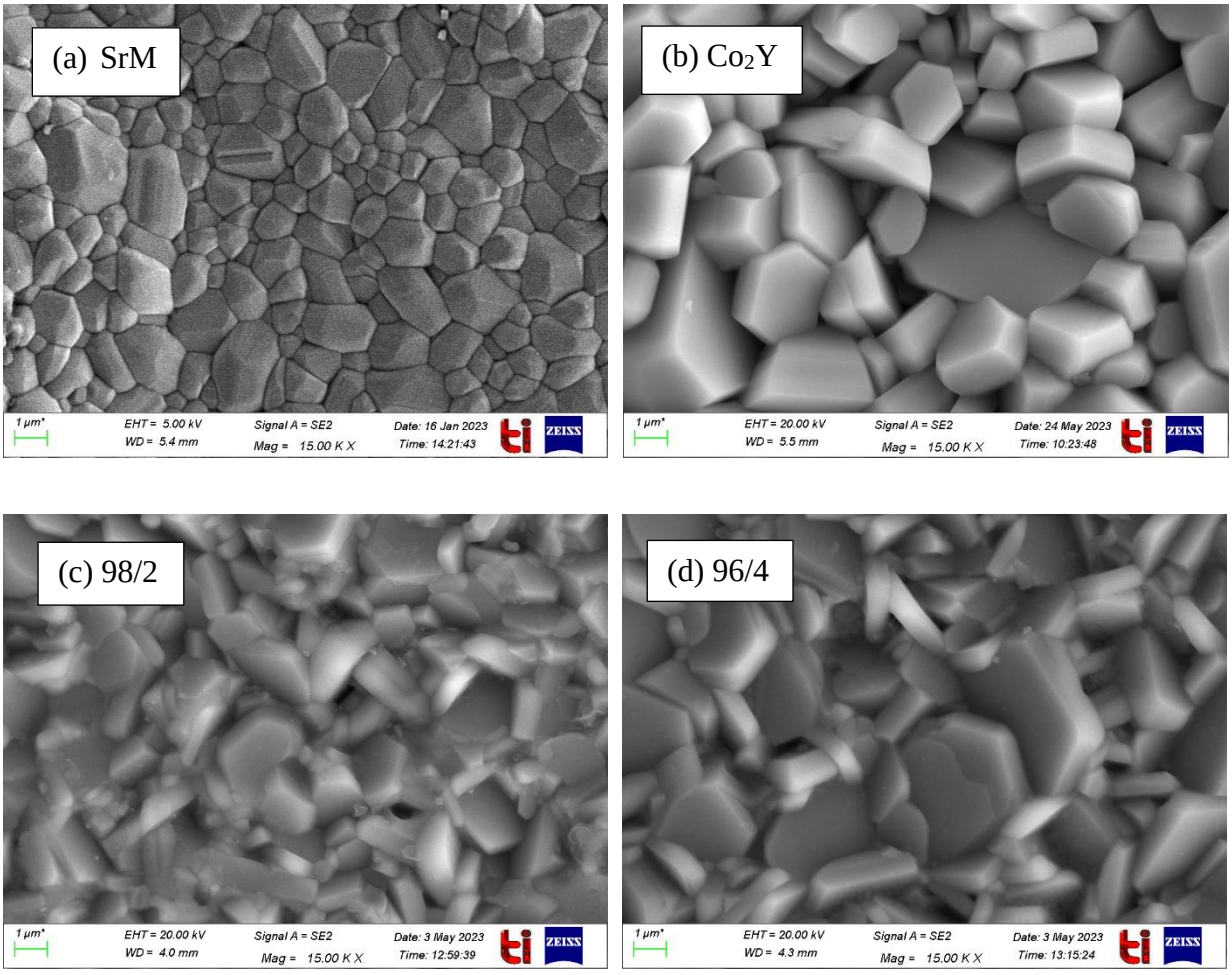

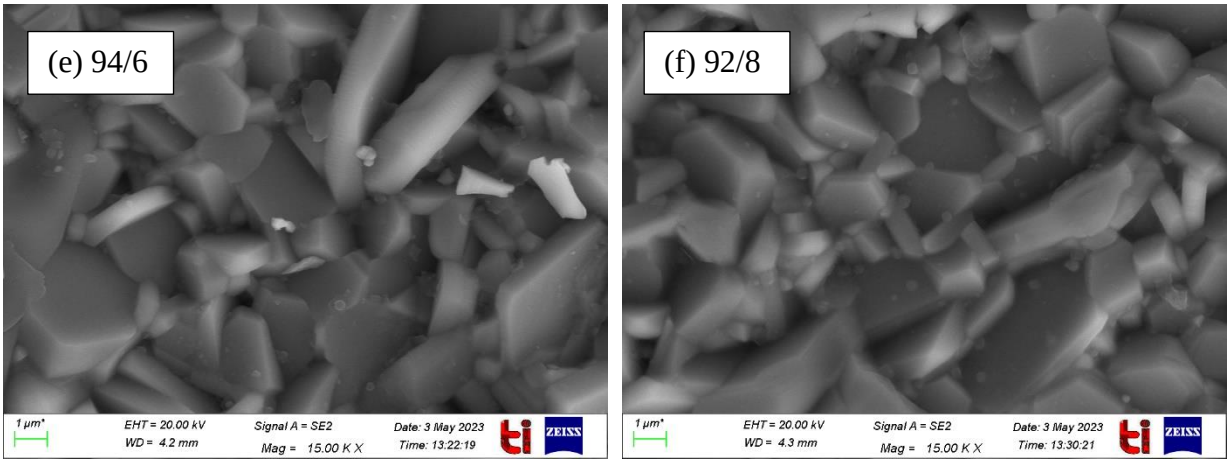

Fig. 4.2 SEM images of (a) SrM, (b) Co_2Y and (c-f) SrM/Co_2Y composites in different weight ratios

4.3 Raman Spectroscopy

Raman spectroscopy was employed to determine vibrations related with the crystal structure of SrM and Co_2Y hexaferrites. The Raman spectrum of hexaferrites typically exhibits a range of vibrational modes, which can be attributed to different types of lattice vibrations, such as stretching, bending, and rotational motions of the atoms within the crystal lattice.

Fig. 4.3 shows Raman spectra of SrM, Co_2Y, and SrM/Co_2Y composite ferrites within the range of 200 to 800 cm^{-1}. Peak parameters obtained from Lorentzian fits are given in Table 4.1. Group theory treatment yields SrM has 42 Raman active modes ($11A_{1g}+14E_{1g}+17E_{2g}$) and 30 IR-active modes ($13A_{2u}+17E_{1u}$) [46]. All the peaks observed in fig 4.3 (a) agreed with the magnetoplumbite structure as reported in literature[47]. The Raman-active modes at 168 and 183 cm^{-1} correspond to spinel block vibrations with E1g symmetry. Peaks at 409, 472, 617, 688 and 726 cm^{-1} of A_{1g} symmetry associated to 12k, 12k+2a, $4f_2$, 2b and $4f_1$ sites respectively, whereas the peak centered at 341 cm^{-1} of $A_{1g}+E_{1g}$ symmetry assigned to octahedra mixed site. In Y-type hexaferrites the results of a group-theory analysis of the lattice vibrations at the Γ point are as follows[48]:

$$\Gamma = 14A_{1g}\,(a^2 + b^2, c^2) + 4A_{1u}(-) + 4A_{2g}(-) + 16A_{2u}(c) + 18E_g\,(a^2 - b^2, ab, ac, bc) + 20E_u(ab) \quad (2)$$

Raman spectra of Co_2Y barium hexaferrite exhibit modes at 177, 205,244, 284, 317, 368, 405, 459, 492, 599, 614, 634, 666, 699 and 717 cm^{-1} fig. 4.4 (b). The peak at 177 cm^{-1} with E_{1g} symmetry is assigned to spinel block, while the bands at 614, 699 and 717 cm^{-1} with A1g symmetry are assigned to 4f2, 2b and 4f1 sites respectively. To the best of our knowledge, there is minimal literature on Y-type hexaferrite Raman spectroscopy[49]. The Raman spectra of SrM/Co_2Y composites shows a dominant peak at 689 cm^{-1} fig. 4.3 (c-f) corresponding to SrM hexaferrite. However, the Co_2Y peak was not visible in the composites this could be due to the low concentration of Y-type content; as the Raman intensity is depending on the materials concentration.

Table 4.1: Band assignment and Raman shift from fitted spectra of SrM/Co_2Y composite ferrite

Peak	Symmetry	SrM	Co_2Y	98/2	96/4	94/6	92/8
			130				
Spinel block	E1g	168	177	172	172	171	171
Spinel block	E1g	183		184	183	183	184
	E1g	214	205	210	208	209	210
		236					
	E1g		244				
	E1g	284	284	285	287	284	285
	E2g	320	317	319	318	318	320
Octahedra mixed	A1g+E1g	341		341	340	339	341
--	--	356		358	356	355	352
	E1g		368				
		381		381	381	380	--
	A1g		405				
12k (dominated)	A1g	409		410	409	409	411
--	E2g	428		427	426	425	425
			459				
12k+2a	A1g	472		473	471	471	472
	A1g		492				
--	E2g	533		533	533	532	534
			599				
4f2	A1g	617	614	618	617	616	618
			634				
			666				
2b	A1g	688	699	689	688	687	690
4f1	A1g	726	717	727	727	726	725

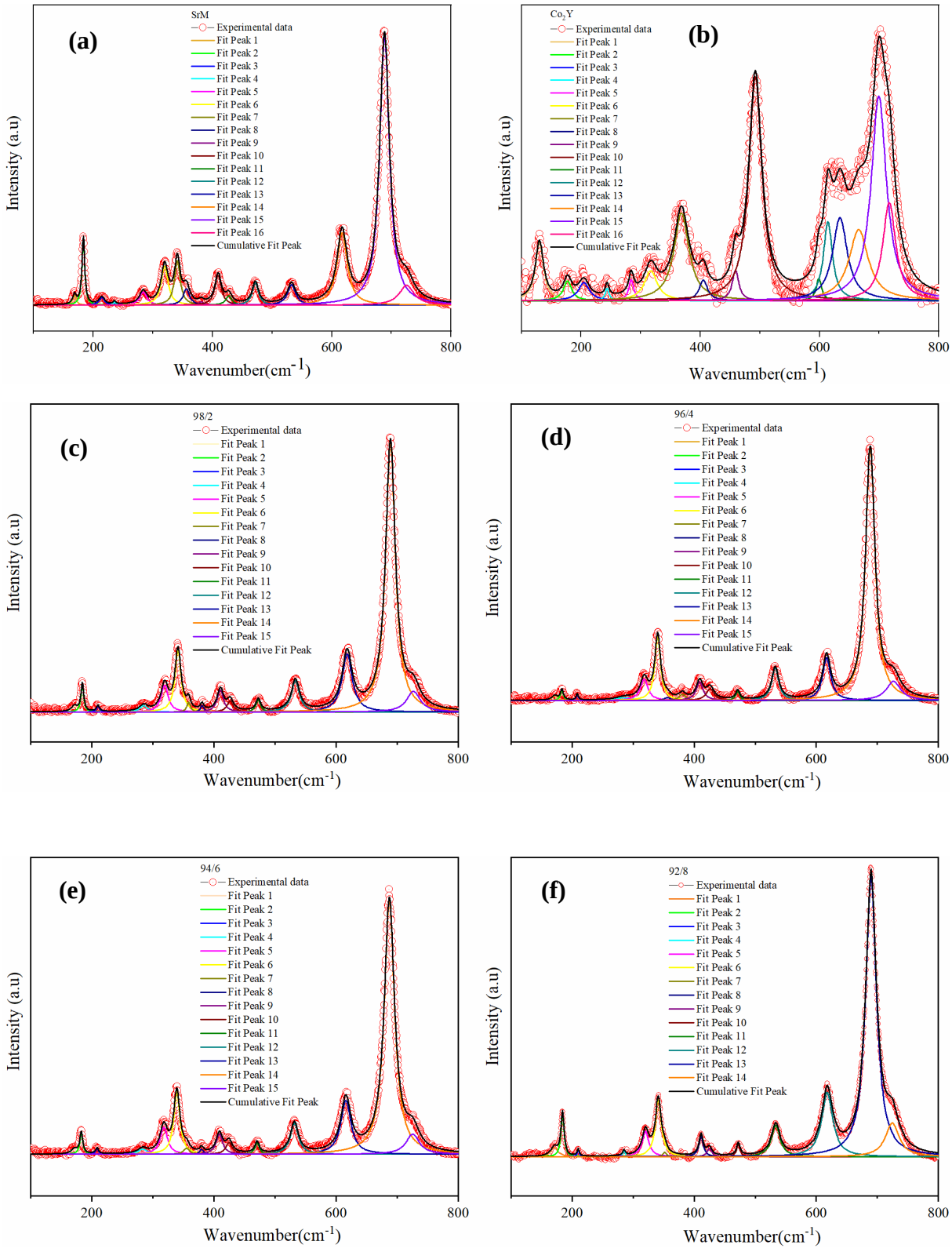

Fig. 4.3 Raman spectra for (a) SrM, (b) Co_2Y and (c-f) SrM/Co_2Y composite at different weight ratios.

4.4 Magnetic measurements

The room temperature *M-H* loop of SrM, Co_2Y, and SrM/Co_2Y composite ferrites are shown in fig. 4.4 (a & b). A non-saturated magnetization curve of SrM is observed, which requires a higher applied field to saturate. A very high coercivity and magnetization at 1 tesla represent the characteristic of hard magnets. The *M-H* loop of Co_2Y is well saturated verifies its in-plane low magneto-crystalline anisotropy and depicts the properties of soft magnets.

The *M-H* loop of as-prepared composites of different composition exhibited smooth demagnetization curve (second quadrant) similar to single-phase hysteresis loop, confer to good exchange coupling between M-Y ferrite. The kink observed in as-mixed composite (inset 4.4 (b)) represents non-exchange couple system. The observed magnetic parameters are tabulated in table 4.2.

To confirm exchange coupling between composites single field distribution (SFD) curves were plotted. The obtained single peak in SFD curve fig 4.5 indicates strong coupling between M-Y ferrite corresponds to coherent switching of both phases with applied field. On the other hand, SFD curve (inset 4.5) of non-exchange coupled composite contains two distinct peaks; indicating individual switching of both phases with applied field.

Table 4.2: Magnetic properties of SrM, Co_2Y and SrM/Co_2Y composites

Magnetic Properties	**SrM/Co_2Y weight ratio**					
	SrM	98/2	96/4	94/6	92/8	Co_2Y
M_s (emu/g)	54.4	55.5	55.6	55.1	55.8	27.92
H_c (Oe)	3461.2	2021.6	1750	1613.8	1416.2	231.4
M_r(emu/g)	33.7	33.2	30.9	29.8	27.2	14.3

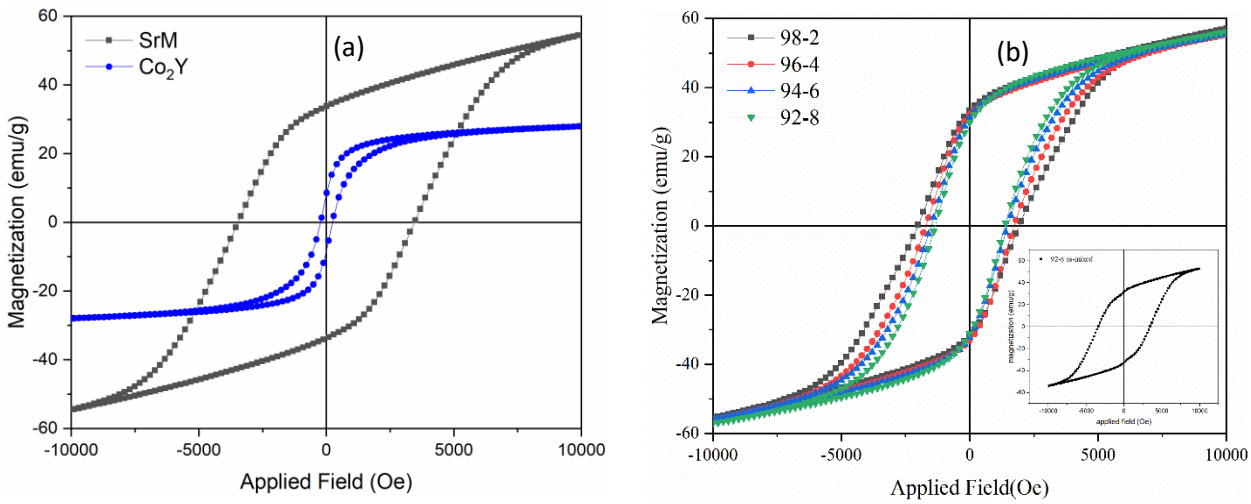

Fig. 4.4 *M-H* loops of (a) SrM & Co_2Y, and (b) sintered SrM/Co_2Y composites in different weight ratios (inset shows *M-H* loop of as-mixed SrM/Co_2Y (92/8) composite)

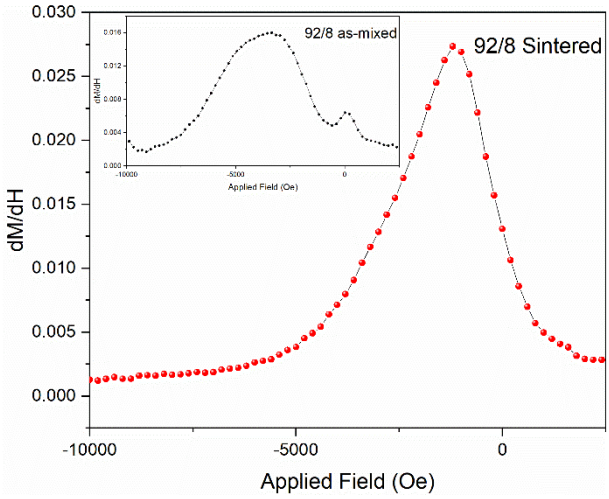

Fig. 4.5 dM/dH *vs* applied field curve of exchange-coupled SrM/Co_2Y (92/8) sintered composite; inset represents dM/ dH *vs* applied field curve of non-exchange coupled composite.

Fig. 4.6 (a & b) depicts the change in M_s and H_c with Co_2Y content in composites. Theoretical values for M_s and H_c were computed using the rule of mixture and compared to experimental results:

$$M_c = (1\text{-}x)M_{1T}SrM + xM_{1T}Co_2Y \quad (1)$$

where, $M_{1T}SrM$ and $M_{1T}Co_2Y$ represents M_s of SrM (54.4 emu/g) and Co_2Y (27.92 emu/g) respectively. Similarly, H_c of the composites was computed and compared to experimental values for varied Co_2Y weight content.

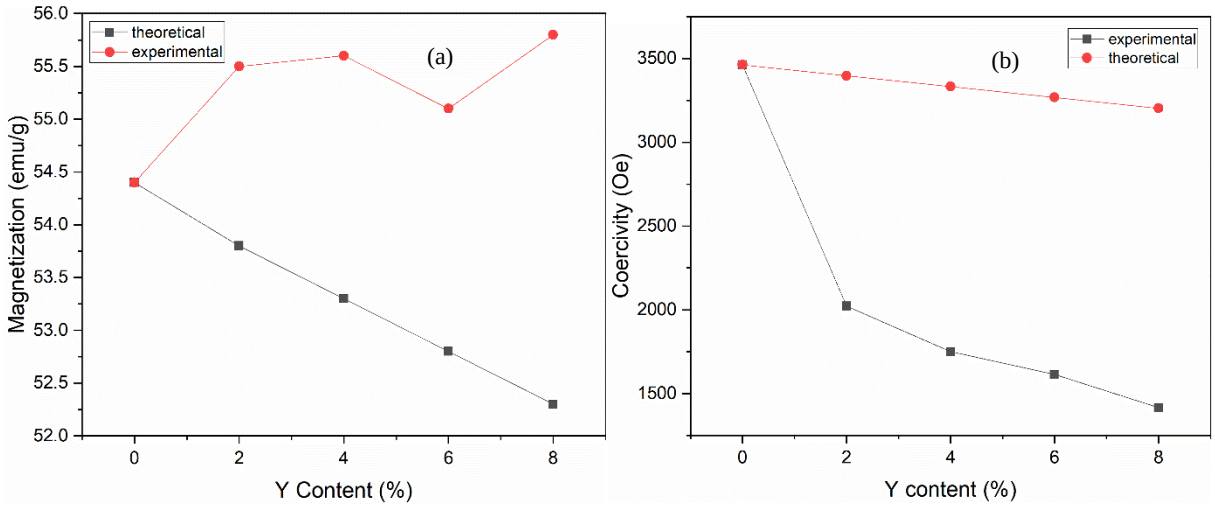

Fig. 4.6 Variation in theoretical and experimental observed (a) *Ms* and (b) *Hc* of SrM/Co_2Y composites with Co_2Y content

According to fig. 4.6 (a), the theoretical M_s of the composite decreases with the Co_2Y content. However experimentally, M_s of the composites increases with Y content this could be due to well interfacial coupling among M-type and Y-type phases as confirmed by demagnetization curve. Moreover, in SrM major fraction of spins are aligned in the field direction but due to grain boundary hinderance there are some spins which requires larger field or an additional driving force

to make them align in field direction. With addition of Co_2Y phase due to its soft magnetic nature spins gets quickly align at much lower magnetic fields as it provides torque to hindered spins [43]. Consequently, a higher percentage of spin alignment raises the magnetization. Further in SrM/Co_2Y composite having 94/6 weight ratio shows declination in M_s value as compared to other compositions which might occur due to the weak coupling between both phases.

On the contrary, H_c of the composites found to decrease fig. 4.6 (b) with Y content due to strong interfacial coupling between the phases where switching of Co_2Y magnetic spins at low nucleation field drive away the hard magnetic spins. The obtained results shows that magnetic properties of composites are Y-phase dependent.

Conclusion

The SrM/Co_2Y composites in different weight ratios (98/2,96/4,94/6,92/8) were successfully synthesized by physical mixing of individual SrM and Co_2Y powder. The impact of relative weight ratio on structural, morphological, and magnetic properties was studied. XRD pattern shows the coexistence of both phases which is also confirmed by Raman analysis. Magnetic property analysis at room temperature revealed smooth *M-H* loop which confirms the well exchange coupling in composites. Experimental M_s of composites found to be higher than both the phase, which further suggest the existing of interfacial coupling among the phase. An initial sharp decrease followed by linear decrease in coercivity was observed with the increasing Y content.

References

[1] J. Jacob, M.A. Khadar, A. Lonappan, K.T. Mathew, Microwave dielectric properties of nanostructured nickel ferrite, Bull. Mater. Sci. 31 (2008) 847–851. https://doi.org/10.1007/s12034-008-0135-9.

[2] N. Laboratorium, E. Nederland, DISPERSION AND ABSORPTION IN MAGNETIC F E R R I T E S A T F R E Q U E N C I E S A B O V E O N E Mc/s by J. L. SNOEK, (1948).

[3] S.C. Tolani, A.R. Golhar, K.G. Rewatkar, A review of morphological, structural behaviour and technological applications of ferrites, AIP Conf. Proc. 2104 (2019). https://doi.org/10.1063/1.5100459.

[4] S.F. Shaikh, M. Ubaidullah, R.S. Mane, A.M. Al-Enizi, Types, Synthesis methods and applications of ferrites, Elsevier Inc., 2020. https://doi.org/10.1016/b978-0-12-819237-5.00004-3.

[5] R. Valenzuela, Novel applications of ferrites, Phys. Res. Int. 2012 (2012). https://doi.org/10.1155/2012/591839.

[6] V.G. Harris, A. Geiler, Y. Chen, S.D. Yoon, M. Wu, A. Yang, Z. Chen, P. He, P. V. Parimi, X. Zuo, C.E. Patton, M. Abe, O. Acher, C. Vittoria, Recent advances in processing and applications of microwave ferrites, J. Magn. Magn. Mater. 321 (2009) 2035–2047. https://doi.org/10.1016/j.jmmm.2009.01.004.

[7] V.G. Harris, Modern microwave ferrites, IEEE Trans. Magn. 48 (2012) 1075–1104. https://doi.org/10.1109/TMAG.2011.2180732.

[8] J.C. Guzmán-Mínguez, L.M. Vicente-Arche, C. Granados-Miralles, J.F. Fernández, A.

Quesada, Improvement of the magnetic properties of SrFe12O19 ceramics by tailored sintering with SiO2 addition, J. Alloys Compd. 860 (2021). https://doi.org/10.1016/j.jallcom.2020.157890.

[9] S.K. Chawla, R.K. Mudsainiyan, S.S. Meena, S.M. Yusuf, Sol-gel synthesis, structural and magnetic properties of nanoscale M-type barium hexaferrites BaCoxZrxFe(12-2x)O 19, J. Magn. Magn. Mater. 350 (2014) 23–29. https://doi.org/10.1016/j.jmmm.2013.09.007.

[10] S.A. Mathews, D.R. Babu, Analysis of the role of M-type hexaferrite-based materials in electromagnetic interference shielding, Curr. Appl. Phys. 29 (2021) 39–53. https://doi.org/10.1016/j.cap.2021.06.001.

[11] R.B. Jotania, H.S. Virk, Y-type hexaferrites: Structural, dielectric and magnetic properties, Solid State Phenom. 189 (2012) 209–232. https://doi.org/10.4028/www.scientific.net/SSP.189.209.

[12] R.C. Pullar, Hexagonal ferrites: A review of the synthesis, properties and applications of hexaferrite ceramics, Prog. Mater. Sci. 57 (2012) 1191–1334. https://doi.org/10.1016/j.pmatsci.2012.04.001.

[13] C.B. Park, K.W. Shin, S.H. Chun, J.H. Lee, Y.S. Oh, S.M. Disseler, C.A. Heikes, W.D. Ratcliff, W.S. Noh, J.H. Park, K.H. Kim, Control of magnetoelectric coupling in the Co2 y -type hexaferrites, Phys. Rev. Mater. 5 (2021) 1–9. https://doi.org/10.1103/PhysRevMaterials.5.034412.

[14] B. Yang, Z. Ji, G. Zhilun, L. Longtu, Magnetic properties of non-stoichiometric Y-type hexaferrite, J. Magn. Magn. Mater. 250 (2002) 364–369. https://doi.org/10.1016/S0304-

8853(02)00420-1.

[15] J.P. Liu, Y. Liu, R. Skomski, D.J. Sellmyer, :: M, 35 (1999) 3241–3246.

[16] E.F. Kneller, R. Hawig, The exchange-spring magnet: A new material principle for permanent magnets, IEEE Trans. Magn. 27 (1991) 3588–3600. https://doi.org/10.1109/20.102931.

[17] V.M. Chakka, Z.S. Shan, J.P. Liu, Effect of coupling strength on magnetic properties of exchange spring magnets, J. Appl. Phys. 94 (2003) 6673–6677. https://doi.org/10.1063/1.1621712.

[18] H. Yang, T. Ye, Y. Lin, M. Liu, Exchange coupling behavior and microwave absorbing property of the hard/soft (BaFe12O19/Y3Fe5O12) ferrites based on polyaniline, Synth. Met. 210 (2015) 245–250. https://doi.org/10.1016/j.synthmet.2015.10.006.

[19] D. Roy, C. Shivakumara, P.S. Anil Kumar, Observation of the exchange spring behavior in hard-soft-ferrite nanocomposite, J. Magn. Magn. Mater. 321 (2009) 12–15. https://doi.org/10.1016/j.jmmm.2008.09.017.

[20] F. Licci, G. Turilli, T. Besagni, Phase Analysis and Single Domain Detection in Hexaferrite Powders for Magnetic Recording., IEEE Trans. Magn. 24 (1987) 593–597. https://doi.org/10.1109/20.43989.

[21] M. Pardavi-Horvath, Microwave applications of soft ferrites, J. Magn. Magn. Mater. 215 (2000) 171–183. https://doi.org/10.1016/S0304-8853(00)00106-2.

[22] C.S. Pawar, M.P. Gujar, V.L. Mathe, Optical Properties of Spin-Deposited Nanocrystalline Ni-Zn Ferrite Thin Films Processed by Sol-Gel, J. Supercond. Nov.

Magn. 30 (2017) 615–625. https://doi.org/10.1007/s10948-016-3720-y.

[23] R.S. Joshi, P.S.A. Kumar, Magnetic Solid-State Materials, Elsevier Ltd., 2013. https://doi.org/10.1016/B978-0-08-097774-4.00413-7.

[24] Z. Jin, W. Tang, J. Zhang, H. Lin, Y. Du, Magnetic properties of isotropic SrFe12O19 fine particles prepared by mechanical alloying, J. Magn. Magn. Mater. 182 (1998) 231–237. https://doi.org/10.1016/S0304-8853(97)00679-3.

[25] M.N. Ashiq, M.J. Iqbal, I.H. Gul, Structural, magnetic and dielectric properties of Zr-Cd substituted strontium hexaferrite (SrFe12O19) nanoparticles, J. Alloys Compd. 487 (2009) 341–345. https://doi.org/10.1016/j.jallcom.2009.07.140.

[26] E. Roohani, H. Arabi, R. Sarhaddi, S. Sudkhah, M-Type Strontium Hexaferrite Nanoparticles Prepared by Sol-Gel Auto-combustion Method: The Role of Co Substitution in Structural, Morphological, and Magnetic Properties, J. Supercond. Nov. Magn. 30 (2017) 1599–1608. https://doi.org/10.1007/s10948-016-3966-4.

[27] C. Liu, X. Kan, F. Hu, X. Liu, S. Feng, J. Hu, W. Wang, K.M. Ur Rehman, M. Shezad, C. Zhang, H. Li, S. Zhou, Q. Wu, Characterizations of magnetic transition behavior and electromagnetic properties of Co-Ti co-substituted SrM-based hexaferrites SrCoxTixFe12-2xO19 compounds, J. Alloys Compd. 784 (2019) 1175–1186. https://doi.org/10.1016/j.jallcom.2019.01.112.

[28] A. Gholizadeh, V. Banihashemi, Effects of Ca–Gd co-substitution on the structural, magnetic, and dielectric properties of M-type strontium hexaferrite, J. Am. Ceram. Soc. (2023). https://doi.org/10.1111/jace.19191.

[29] S. Kumar Godara, Nomita, V. Kaur, A.K. Srivastava, D. Basandrai, J. Ahmed, J. Mohammed, M. Singh, P. Kaur, A. Mehtab, T. Ahmad, R. Kumar Dhaka, P.K. Maji, A. Kumar Sood, Effect on Magnetic, morphological and structural properties of Zn2+-Zr4+ substituted SrM for permanent magnet based appliances, J. Magn. Magn. Mater. 560 (2022) 169626. https://doi.org/10.1016/j.jmmm.2022.169626.

[30] J.Y. Choi, Y.K. Baek, J.G. Lee, Y.K. Kim, Effect of sodium addition on structural and magnetic properties of solid state processed SrFe12−xAlxO19 (x ≤ 4), Appl. Phys. A Mater. Sci. Process. 128 (2022) 1–9. https://doi.org/10.1007/s00339-022-06238-w.

[31] X. Yu, N. Zhou, R. Liu, L. Wang, Z. Xu, H. Gong, T. Zhao, J. Sun, F. Hu, B. Shen, Effect of Zn2+-Sn4+ co-substitution on structural and magnetic properties of SrFe12-2xZnxSnxO19 (x = 0–2) M-type strontium ferrite, Phys. B Condens. Matter. 653 (2023) 414676. https://doi.org/10.1016/j.physb.2023.414676.

[32] Y. Bai, J. Zhou, Z. Gui, L. Li, Magnetic properties of Cu, Zn-modified Co2Y hexaferrites, J. Magn. Magn. Mater. 246 (2002) 140–144. https://doi.org/10.1016/S0304-8853(02)00040-9.

[33] N. Chand Pramanik, T. Fujii, M. Nakanishi, J. Takada, S.I. Seok, The effect of heat treatment temperature on the microstructure and magnetic properties of Ba2Co2Fe12O22 (Co2Y) prepared by sol-gel method, Mater. Lett. 60 (2006) 2718–2722. https://doi.org/10.1016/j.matlet.2006.01.077.

[34] M.M. Costa, G.F.M. Pires, A.J. Terezo, M.P.F. Graa, A.S.B. Sombra, Impedance and modulus studies of magnetic ceramic oxide Ba 2Co2Fe12O22 (Co2Y) doped with Bi2O3, J. Appl. Phys. 110 (2011). https://doi.org/10.1063/1.3615935.

[35] M.M. Rashad, D.A. Rayan, M. EL-Gendy, M.M. El Kholy, T.A. Taha, Structural and Magnetic Characteristics of Ferroxplana Co2Y Nanoferrites Synthesized via Two Chemical Routes, J. Supercond. Nov. Magn. 31 (2018) 4191–4198. https://doi.org/10.1007/s10948-018-4674-z.

[36] R. Vinaykumar, Jyoti, J. Bera, Characterization of La-Zn Substituted Co2Y Hexagonal Ferrite, J. Electron. Mater. 47 (2018) 5959–5964. https://doi.org/10.1007/s11664-018-6486-0.

[37] G. Packiaraj, K. Sakthipandi, R.B. Jotania, A. Hossain, Dielectric and Magnetic Properties of Polyaniline-Blended Y-Type Ba2Ni2Fe12O22 Hexaferrite Composites, J. Electron. Mater. 49 (2020) 3317–3324. https://doi.org/10.1007/s11664-020-08051-8.

[38] Y. Gao, Q. Wu, J. Song, Q. Man, Achieving broad absorption bandwidth of Ba2Co2Fe12O22 ferrites by adjusting the sintering temperature, J. Magn. Magn. Mater. 554 (2022) 169312. https://doi.org/10.1016/j.jmmm.2022.169312.

[39] X. Liu, W. Zhong, B. Gu, Y. Du, Exchange-coupling interaction in nanocomposite SrFe 12O 19/γ-Fe 2O 3 permanent ferrites, J. Appl. Phys. 92 (2002) 1028–1032. https://doi.org/10.1063/1.1487908.

[40] L. Zhang, Z. Li, Synthesis and characterization of SrFe12O19/CoFe2O4 nanocomposites with core-shell structure, J. Alloys Compd. 469 (2009) 422–426. https://doi.org/10.1016/j.jallcom.2008.01.152.

[41] S.R. Saeedi Afshar, M. Hasheminiasari, S.M. Masoudpanah, Structural, magnetic and microwave absorption properties of SrFe12O19/Ni0.6Zn0.4Fe2O4 composites prepared by one-pot solution combustion method, J. Magn. Magn. Mater. 466 (2018) 1–6.

https://doi.org/10.1016/j.jmmm.2018.06.061.

[42] F. Mohseni, R.C. Pullar, J.M. Vieira, J.S. Amaral, Enhancement of maximum energy product in exchange-coupled BaFe12O19/Fe3O4 core-shell-like nanocomposites, J. Alloys Compd. 806 (2019) 120–126. https://doi.org/10.1016/j.jallcom.2019.07.162.

[43] C. Pahwa, S.B. Narang, P. Sharma, Composition dependent magnetic and microwave properties of exchange-coupled hard/soft nanocomposite ferrite, J. Alloys Compd. 815 (2020) 152391. https://doi.org/10.1016/j.jallcom.2019.152391.

[44] P. Maltoni, T. Sarkar, G. Barucca, G. Varvaro, D. Peddis, R. Mathieu, Exploring the magnetic properties and magnetic coupling in SrFe12O19/Co1-xZnxFe2O4 nanocomposites, J. Magn. Magn. Mater. 535 (2021) 168095. https://doi.org/10.1016/j.jmmm.2021.168095.

[45] V. Bilovol, M. Sikora, K. Berent, Exchange coupling in SrFe12O19/CoFe2O4 composites: Effect of component proportions, J. Magn. Magn. Mater. 568 (2023) 170384. https://doi.org/10.1016/j.jmmm.2023.170384.

[46] Q. Wu, Z. Yu, H. Hao, Y. Chu, H. Xie, The effect of pH value on strontium hexaferrites: microstructure and magnetic properties, J. Mater. Sci. Mater. Electron. 28 (2017) 12768–12775. https://doi.org/10.1007/s10854-017-7104-2.

[47] J. Kreisel, G. Lucazeau, H. Vincent, Raman Spectra and Vibrational Analysis of BaFe12O19Hexagonal Ferrite, J. Solid State Chem. 137 (1998) 127–137. https://doi.org/10.1006/jssc.1997.7737.

[48] T. Tchouank Tekou Carol, J. Mohammed, D. Basandrai, S.K. Godara, G.R. Bhadu, S.

Mishra, N. Aggarwal, S.B. Narang, A.K. Srivastava, X-band shielding of electromagnetic interference (EMI) by Co2Y barium hexaferrite, bismuth copper titanate (BCTO), and polyaniline (PANI) composite, J. Magn. Magn. Mater. 501 (2020) 1–12. https://doi.org/10.1016/j.jmmm.2020.166433.

[49] M. Manendar, S.S.K. Reddy, J. Ramesh, M.S. Reddy, M.M. Raja, C.G. Reddy, P.Y. Reddy, V.R. Reddy, Cation distribution in Ni substituted Ba0.5Sr1.5Co2Fe12O22 Y-type hexagonal ferrites, Ceram. Int. 47 (2021) 9591–9596. https://doi.org/10.1016/j.ceramint.2020.12.094.